Article
Chinese Science Bulletin
Geology
September 2012 Vol.57 No.26: 3482–3490
doi: 10.1007/s11434-012-5176-1

Closure temperature of (U-Th)/He system in apatite obtained from natural drillhole samples in the Tarim basin and its geological significance

CHANG Jian[1,2] & QIU NanSheng[1,2*]

[1] *State Key Laboratory of Petroleum Resource and Prospecting, China University of Petroleum, Beijing 102249, China;*
[2] *Basin and Reservoir Research Center, China University of Petroleum, Beijing 102249, China*

Received February 27, 2012; accepted March 27, 2012; published online May 15, 2012

The apatite (U-Th)/He thermochronometry has been used to study the tectono-thermal evolution of mountains and sedimentary basins for over ten years. The closure temperature of helium is important for the apatite (U-Th)/He thermochronometry and has been widely studied by thermal simulation experiments. In this paper, the apatite He closure temperature was studied by establishing the evolutionary pattern between apatite He ages and apatite burial depth based on examined apatite He ages of natural samples obtained from drillholes in the Tarim basin, China. The study showed that the apatite He closure temperature of natural samples in the Tarim basin is approximately 88±5°C, higher than the result (~75°C) obtained from the thermal simulation experiments. The high He closure temperature resulted from high effective uranium concentration, long-term radiation damage accumulation, and sufficient particle radii. This study is a reevaluation of the conventional apatite He closure temperature and has a great significance in studying the uplifting events in the late period of the basin-mountain tectonic evolution, of which the uplifting time and rates can be determined accurately.

apatite He closure temperature, effective uranium concentration (eU), radiation damage, particle radii, Tarim basin

Citation: Chang J, Qiu N S. Closure temperature of (U-Th)/He system in apatite obtained from natural drillhole samples in the Tarim basin and its geological significance. Chin Sci Bull, 2012, 57: 3482–3490, doi: 10.1007/s11434-012-5176-1

The (U-Th)/He thermochronometry is based on measuring the accumulation of radiogenic ^{4}He produced by the decay of U and Th in apatite, zircon and other minerals and has been widely applied in several research fields, such as the landscape evolution, thermal evolution of sedimentary basins, hydrocarbon and mineral exploration and geodynamic evolution of cratons. The closure temperature was firstly proposed by the Dodson in 1973 [1], and then applied to the K-Ar, Ar-Ar, fission track and (U-Th)/He thermochronological systems. Thermal simulation experiments suggested that the (U-Th)/He closure temperature of apatite was ~75°C [2–4], which has been used to study the thermal evolution of sedimentary basins. However, it is found that there are significant differences on the apatite He closure temperatures determined by He ages of the natural samples in the sedimentary basins [5–7]. In the German Continental Deep Drilling (KTB), the He closure temperature of the fluorapatite was 90±22°C, whereas the Cl and OH^{-}-rich apatite trend towards lower closure temperatures on the order of 55±30°C [5]; The apatite He closure temperature of the Otway basin in Australia was about 75°C [6]. Some studies suggested that the apatite He closure temperature varies with the cooling time, the effective uranium concentration (eU), radiation damage, particle radii and the F/Cl ratio [8–12]. Recently, we have discovered that thermal histories simulated by apatite He ages using the He closure temperature of the thermal simulation experiments disagreed with actual geological condition in the Tarim basin [13–15], contrary to the study result on tectono-thermal evolution of the Tarim basin. Correctly understanding the

*Corresponding author (email: qiunsh@cup.edu.cn)

apatite He closure temperature in a region not only reveals the correct geological information involved in the examined He ages but also provides a basis for related future research. In this paper, we derived the apatite He closure temperature of the Tarim basin from evolutionary pattern between the apatite He ages and burial depths based on the examined apatite He ages of the natural samples obtained from drilling wells in the Tarim basin. This study is a reevaluation of the conventional apatite He closure temperature and has a great significance in determining the time and rate of the basin-mountain uplift.

1 Samples and experiments

The samples were collected from the Tarim basin, China (Figure 1). The apatite He closure temperature of natural samples is usually calculated by establishing the evolutionary pattern between apatite He ages and apatite depth; hence, the apatite must reach the current maximum temperature after deposition. Therefore, samples should be collected from an area where tectonic movements are few and thick sediments are deposited in the late period, such as the Tabei Uplift, Northern Depression, and Central Uplift in the Tarim basin. The Tabei Uplift, Northern Depression, and Central Uplift have been subsiding since the Mesozoic, and 3000-m-thick sediments have accumulated in these areas (Figure 2). The samples were collected from wells S14, S87, S110, and XH1 in the Tabei Uplift, well Sh1 in the Northern Depression, and wells Z2 and Z11 in the Central Uplift (Figure 3). The details of all samples are given in Table 1.

Apatite grains were separated from the collected samples using conventional mineral separation techniques. The (U-Th)/He analyses were conducted in the Arizona Radiogenic Helium Dating Laboratory (ARHDL) at University of Arizona in America. The experiments primarily consisted of three steps: (1) He extraction and measurement from the apatite grains—the grains inside Nb foil packets were heated with a laser beam to approximately 900–1000°C (the grains were heated for 3 min) to extract ^{4}He. The ^{4}He released from the apatite were then spiked with 0.1–0.2 pmol ^{3}He and condensed at 16 K. The whole helium was then

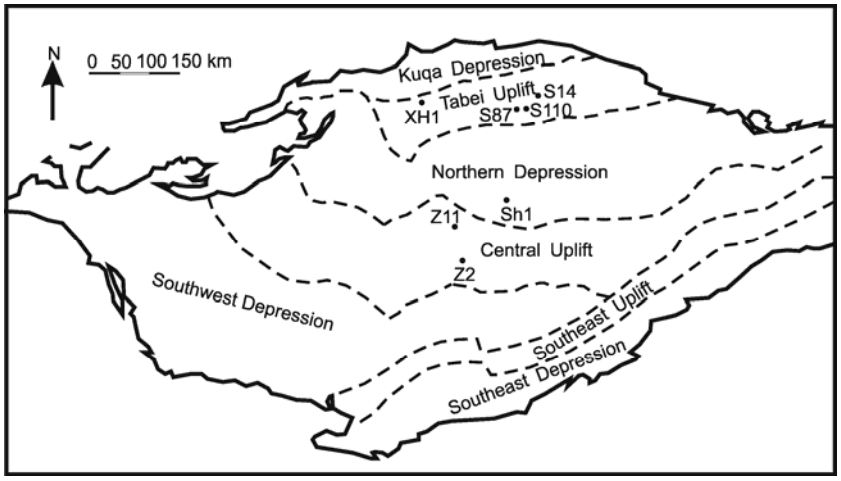

Figure 1 Structural units of the Tarim basin showing the locations of the wells.

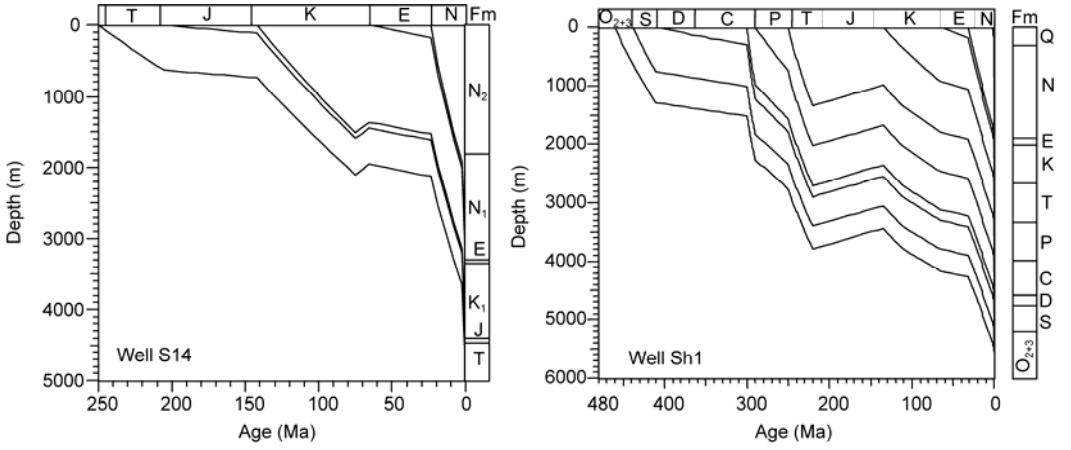

Figure 2 Burial histories of the typical wells in the Tarim basin.

Table 1 The test (U-Th)/He ages of apatite samples in the Tarim basin

Sample No.	Strat.	Litho.	Depth (m)	Radius (μm)	Th/U[a)] (atomic)	Raw age (Ma)	Mass (μg)	U (ppm)	Th (ppm)	Sm (ppm)	F_T [b)]	Corrected age (Ma)	±1σ (Ma)	eU (ppm)	[^{4}He] (nmol/g)
S14-10a1	Cretaceous	sandstone	3680	51	1.06	36.52	4.35	32.95	34.05	32.59	0.730	50.00	0.87	40.95	8.10
S14-10a2	Cretaceous	sandstone	3680	59.6	0.81	1.14	4.41	6.86	5.43	5.05	0.746	1.53	0.18	8.13	0.05
S14-11	Cretaceous	sandstone	4015	48.3	0.65	8.26	2.94	18.91	11.99	115.27	0.708	11.67	0.31	21.73	0.97
S14-12	Cretaceous	sandstone	4274	36	0.64	0.40	1.13	30.37	18.97	89.25	0.640	0.63	0.23	34.83	0.08
S14-14	Triassic	sandstone	4785	40.8	0.83	0.02	2.07	33.52	26.99	233.21	0.667	0.03	0.07	39.86	0.00
S87-1	Triassic	sandstone	4213.5	37.3	1.72	1.26	1.75	4.24	7.12	383.22	0.668	1.89	0.66	5.92	0.04
S87-3	Triassic	sandstone	4721	45.5	0.51	1.99	2.20	9.92	4.91	6.80	0.718	2.77	0.24	11.07	0.12
S87-4	Triassic	sandstone	4829.5	30.8	29.56	0.38	0.73	5.40	155.55	198.75	0.552	0.68	0.27	41.95	0.09
S87-7	Carboniferous	sandstone	5014.8	43.8	12.87	1.04	2.14	0.38	4.82	7.51	0.688	1.51	1.84	1.52	0.01
S87-9	Carboniferous	sandstone	5233.4	59.3	3.15	0.39	5.32	8.19	25.17	14.81	0.773	0.50	0.09	14.10	0.03
S87-10	Carboniferous	sandstone	5290	31.3	3.68	2.92	0.97	25.54	91.54	615.64	0.601	4.86	0.22	47.05	0.76
S87-11	Carboniferous	sandstone	5502.3	38	3.01	0.53	1.33	20.76	60.92	228.49	0.620	0.85	0.18	35.08	0.1
S87-12	Carboniferous	sandstone	5510	41.5	3.06	0.49	1.85	14.92	44.50	363.03	0.652	0.76	0.17	25.38	0.07
S87-13	Ordovician	sandstone	5529.8	52.3	7.40	0.18	3.73	7.93	57.17	118.93	0.710	0.26	0.08	21.36	0.02
S110-2	Triassic	sandstone	4250	36.8	0.26	17.79	1.41	75.06	18.83	66.52	0.668	26.63	0.63	79.48	7.64
S110-3	Triassic	sandstone	4348.8	71.5	10.22	23.66	8.01	2.39	23.77	126.62	0.773	30.60	0.60	7.97	1.04
S110-5	Triassic	sandstone	4426	58.8	3.79	9.38	5.98	4.07	15.03	175.18	0.773	12.14	0.31	7.60	0.40
S110-10	Silurian	sandstone	5459	34.5	0.27	1.24	1.09	30.25	8.00	170.03	0.610	2.04	0.36	32.14	0.22
S110-12	Silurian	sandstone	5495	57	10.32	0.79	3.72	2.76	27.81	151.28	0.715	1.11	0.20	9.30	0.04
S110-13	Ordovician	sandstone	5967.9	34.3	0.88	0.37	0.98	84.41	72.30	294.80	0.596	0.62	0.11	101.40	0.20
XH1-7	Neogene	sandstone	3958	36	13.97	7.01	1.17	0.31	4.27	12.71	0.587	11.94	5.23	1.32	0.05
XH1-11	Eogene	sandstone	4950	43.3	4.72	3.22	2.00	21.12	97.09	310.24	0.658	4.90	0.14	43.94	0.77
XH1-12	Eogene	sandstone	4954.9	50.3	11.74	0.03	3.74	27.78	317.84	674.80	0.703	0.05	0.02	102.47	0.02
XH1-14a1	Cretaceous	sandstone	5603	51	1.16	0.25	3.33	10.46	11.83	249.56	0.717	0.34	0.17	13.24	0.02
XH1-14a2	Cretaceous	sandstone	5603	60.25	0.33	0.36	4.94	73.04	23.46	155.19	0.783	0.46	0.02	78.55	0.15
XH1-15	Cretaceous	sandstone	5609.6	66.8	2.30	2.74	6.48	38.51	86.49	372.87	0.768	3.57	0.07	58.83	0.88
Sh1-3	Triassic	sandstone	2946	36.8	1.89	55.87	1.03	84.38	155.35	387.59	0.601	92.98	1.40	120.89	36.78
Sh1-4a1	Triassic	diorite	3311	41.8	4.15	27.76	2.15	22.62	91.45	185.74	0.659	42.11	0.62	44.11	6.67
Sh1-5a1	Permian	basalt	3462.3	39.3	5.82	33.92	2.27	8.58	48.64	547.76	0.65	52.22	0.79	20.01	3.81
Sh1-5a2	Permian	basalt	3462.3	43.5	4.81	61.13	3.04	14.75	69.15	747.40	0.68	89.72	1.26	31.00	10.60
Sh1-6a1	Permian	tuff	3509.5	48.8	4.77	89.08	3.04	9.52	44.24	485.17	0.72	128.01	1.87	19.92	9.94
Sh1-6a2	Permian	tuff	3509.5	35	6.58	42.52	1.21	16.60	106.49	471.40	0.66	67.62	1.11	41.63	9.74
Sh1-9	Carboniferous	sandstone	4563.5	45.3	0.98	0.72	1.94	71.44	67.94	105.03	0.67	1.06	0.06	87.41	0.34
Sh1-10	Silurian	sandstone	4583.5	46.5	1.62	7.35	2.16	24.01	37.83	106.73	0.68	10.83	0.26	32.90	1.31
Sh1-12	Silurian	sandstone	4961	36.8	1.43	0.12	1.39	7.21	10.07	138.03	0.63	0.19	0.41	9.58	0.01
Sh1-14	Silurian	sandstone	5331.1	71.5	6.32	0.41	6.98	5.11	31.51	182.48	0.77	0.53	0.06	12.52	0.03
Z2-1a1	Cretaceous	sandstone	2085	57.5	0.54	15.81	4.82	11.23	5.87	149.82	0.750	21.08	0.42	12.61	1.09
Z2-1a2	Cretaceous	sandstone	2085	68.3	1.87	47.76	5.61	12.84	23.42	86.67	0.762	62.65	1.04	18.34	4.78
Z2-2a1	Triassic	sandstone	2553	41.8	2.41	168.15	2.36	117.10	275.02	343.39	0.67	251.12	6.95	181.73	167.50
Z2-2a2	Triassic	sandstone	2553	56.3	0.37	158.38	4.15	73.54	26.72	2.65	0.742	213.56	6.17	79.82	69.10
Z2-3a1	Triassic	sandstone	2963	54.8	3.05	96.44	4.20	15.25	45.27	223.76	0.743	132.34	2.05	25.89	13.73
Z2-3a2	Triassic	sandstone	2963	50.8	0.51	76.67	3.37	100.02	49.26	153.42	0.721	106.37	2.10	111.60	46.51
z2-8	Devonian	sandstone	4804	63	4.00	0.56	4.68	8.16	31.85	34.17	0.742	0.75	0.16	15.65	0.05
Z2-9	Silurian	sandstone	4962	51	2.10	0.27	2.45	21.55	44.04	51.78	0.692	0.39	0.17	31.90	0.05
Z2-10	Silurian	sandstone	5138	53.5	1.02	1.28	4.01	12.77	12.67	328.88	0.732	1.76	0.20	15.75	0.11
Z11-4	Carboniferous	sandstone	4181.6	38	0.90	0.07	1.28	134.40	117.31	587.72	0.63	0.10	0.03	161.97	0.06
Z11-5	Devonian	sandstone	4351.5	68	0.92	0.06	6.80	26.03	23.45	77.77	0.78	0.08	0.03	31.54	0.01
Z11-7	Silurian	sandstone	4701.2	33	1.24	0.45	0.96	62.47	75.36	1006.12	0.59	0.77	0.11	80.18	0.20
Z11-8	Silurian	sandstone	4922	35.5	5.10	0.25	1.30	20.99	104.34	154.06	0.60	0.41	0.25	45.51	0.06
Z11-10	Silurian	sandstone	5091	40.8	18.35	0.15	1.97	14.08	251.84	439.02	0.64	0.23	0.10	73.26	0.06

a) The atomic ratio of thorium and uranium in apatite crystal; b) alpha ejection correction [2].

released from cold head at 37 K into a small volume (50 cc) using an activated Zr-Ti alloy getter. Finally, the ^{4}He/^{3}He radio was measured using quadrupole mass spectrometer; (2) U, Th, and Sm measurements—subsequent to the He measurement, the apatite grains were dissolved in dilute (~20%) HNO_3 solution, and certain amounts of ^{229}Th and

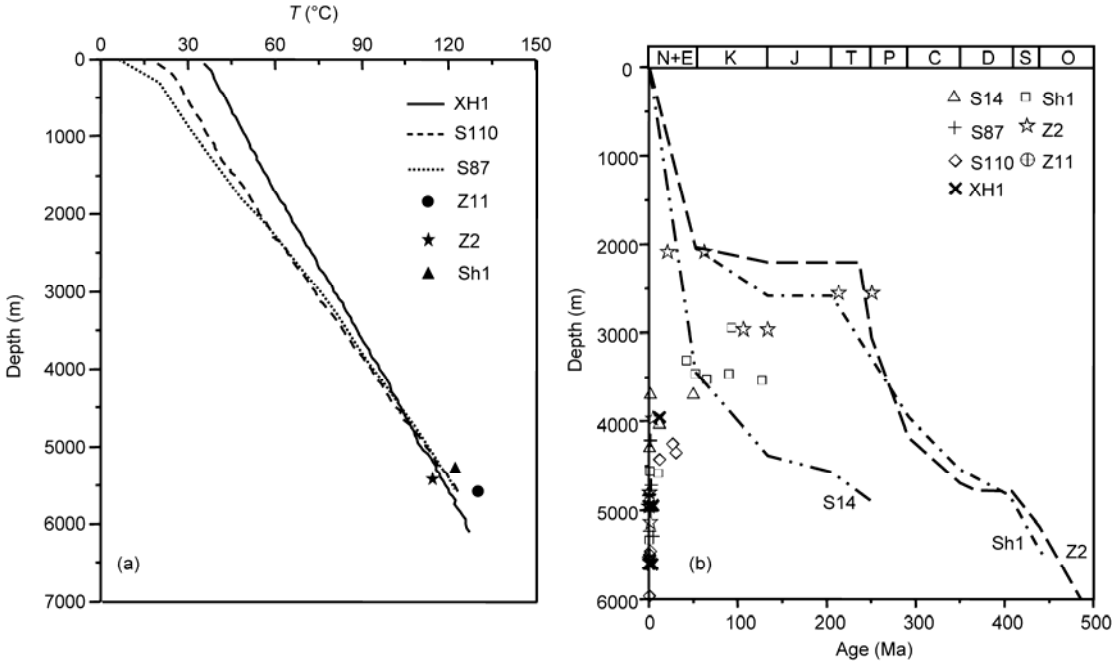

Figure 3 (a) Temperature profiles of the studied wells in the Tarim basin (temperature profiles from well logging for wells S87, S110, and XH1 and oil testing temperatures for wells Sh1, Z2 and Z11); (b) correlation between apatite He ages and burial depths in the Tarim basin (dashed lines represent the stratigraphical ages of wells S14, Z2, and Sh1).

^{233}U solution were added. The final solution was placed into an inductively coupled plasma mass spectrometry, and the ^{238}U/^{233}U and ^{232}Th/^{229}Th ratios were measured to determine the U and Th contents in the apatite grains; (3) Calculation of (U-Th)/He ages—the (U-Th)/He measurement process was described in detail by Reiners [16]. All the test results are listed in Table 1.

2 Apatite He closure temperature in the Tarim basin

The temperature profiles from well logging in wells S87, S110, and XH1 and the temperature data from oil testing in wells Sh1, Z2, and Z11 are plotted against apatite depths, as shown in Figure 3(a). The temperature profile of well S14 was assumed be the same as that of well S110, which is the nearest well, due to lack of temperature data (Figure 1). Samples from wells S14, S87, S110, XH1, and Z11 were buried at depths of more than 3600 m, and their apatite He ages were close to 0 Ma, which indicated that all the helium in the apatite had diffused (Figure 3(b)). Except for the two shallow samples in well Z2, the apatite He ages of the samples from wells Z2 and Sh1 decreased as the burial depth increased and were close to or younger than the deposition ages, which showed that the apatite experienced whole or partial helium diffusion, respectively (Figure 3(b)). Therefore, the apatite He ages of the samples from wells S14, S87, S110, XH1, Sh1, Z2, and Z11 did not reflect the geological information of the source regions but record the information of the research area, which is useful in studying the apatite He closure temperature of the Tarim basin.

The evolutionary patterns between the apatite He ages and apatite depths of wells Z2 and Sh1 are shown in Figure 4. The apatite He closure temperature (T_c) is equal to the temperature at the crossing point between the depth and the tangent line, derived from the evolutionary curve of the apatite He ages (Figure 4). The crossing points of wells Z2 and Sh1 correspond to depths of ~3700 and ~3850 m, respectively. Based on the temperature curves, the apatite He closure temperatures of wells Z2 and Sh1 are ~84 and ~91°C. Subsequently, the evolutionary pattern between the apatite He ages and apatite depths of all seven wells was established (Figure 5). Except for the two shallow samples in well Z2, the apatite He ages of the samples decreased as the burial depth increased and some are close to 0 Ma at 3680 m depth. The crossing point shown in Figure 5 corresponds to a depth of ~3800 m; thus, the apatite He closure temperature in the Tarim basin is 88±5°C (calculated based on the temperature curve shown in Figure 3), which is higher than the result of the thermal simulation experiments [2–4]. Moreover, the partial retention zone of the apatite in the Tarim basin is around 40–88°C (Figure 5).

3 Discussion

Recent studies have discovered that apatite He ages in some cratons are older than the corresponding fission-track ages due to various causes, such as radiation-enhanced annealing,

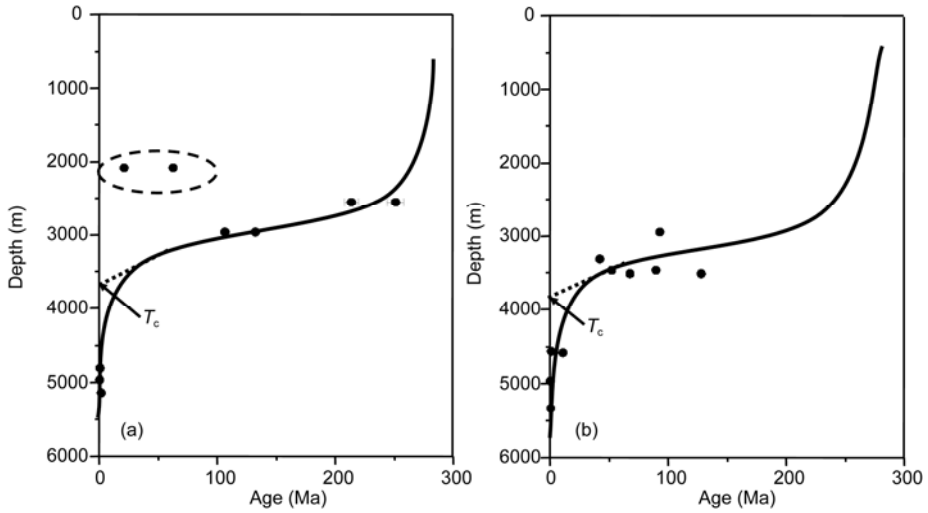

Figure 4 (a) Correlation between apatite He ages and depths in well Z2; (b) correlation between the apatite He ages and depths in well Sh1.

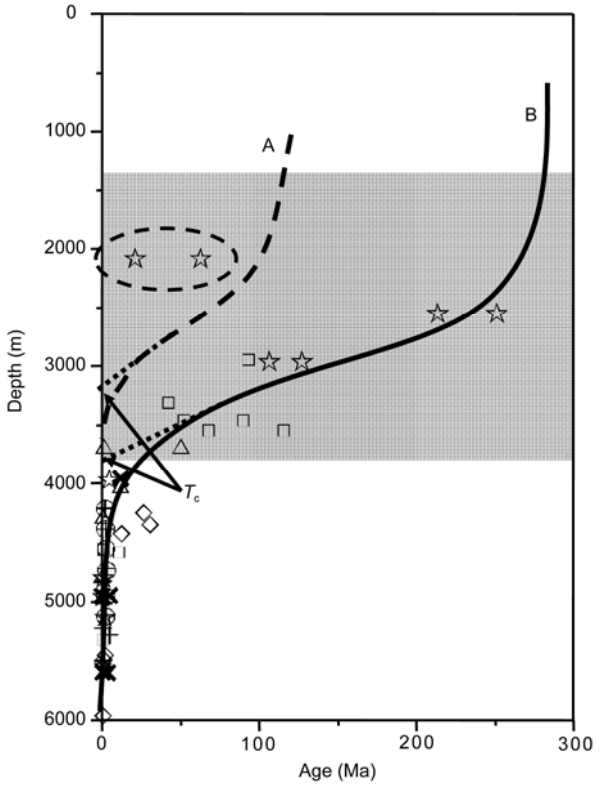

Figure 5 Relationship between the apatite He ages of the studied wells and apatite burial depths in the Tarim basin. Dashed line A is the model from Wolf et al. [3]; solid line B is the model from this study; and the shaded area is the He partial retention zone of the apatite in the Tarim basin.

change in He retention properties, alpha ejection correction, radiation damage, and cooling time [17–20]. The alpha ejection correction of raw (U-Th)/He ages leads to erroneous high ages with respect to relatively slow-cooling apatite [20]. The radiation damage accumulation and annealing model proposed by Flowers et al. [8] can explain some cases where the apatite He ages are older than the corresponding fission track ages. The cases where the apatite He closure temperature is higher than the corresponding fission-track closure temperature are shown in Figure 6. The present study shows that the apatite He closure temperature of the Tarim basin, as a typical cratonic basin, is comparatively high but still lower than the corresponding fission-track closure temperature. Thus, the apatite He age is younger than the corresponding fission-track age in the same stratum [15]. The next sections discuss the causes that resulted in high apatite He closure temperature of the Tarim basin.

3.1 Particle radii

Apatite He diffusion often follows the simple Arrhenius equation, i.e.

$$D / a^2 = D_0 / a^2 \mathrm{e}^{-E_a/RT}, \quad (1)$$

where D is the diffusion coefficient at absolute temperature

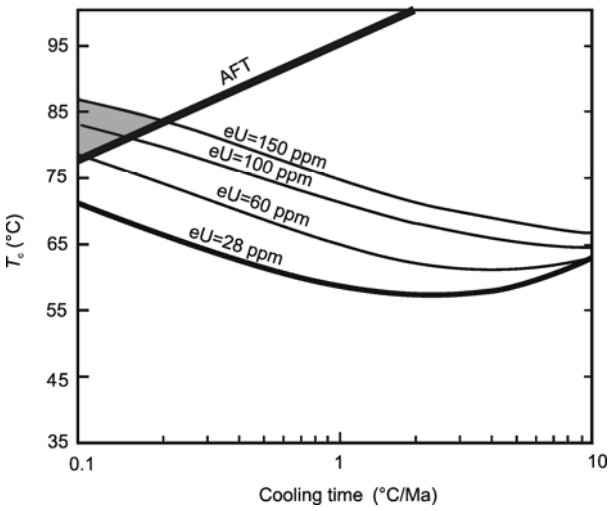

Figure 6 Apatite He closure temperature as a function of cooling time and eU [8]. The He closure temperature is higher than the fission-track closure temperature for the apatite in the shaded area.

T, D_0 represents the diffusion coefficient at infinitely high temperature, E_a is the activation energy for the diffusion process, R is the gas constant, and a is the grain size. The Arrhenius equation indicates that He diffusion is related to the apatite grain size. The alpha-stopping distance is significant to the apatite (U-Th)/He geochronology and is computed from the parent nuclide (U, Th) to the rest site of the alpha particle (^{4}He) during the alpha decay, which ranges from a minimum of ~11 μm to a maximum of ~34 μm [2]. Farley et al. [2,4] not only discussed the three relevant possibilities between the alpha-stopping distances and He retention but also created a function of the grain radius and the He retention. The function is expressed as

$$F_T = 1 - \frac{3S}{4R} + \frac{S^3}{16R^3}, \quad (2)$$

where F_T is the ^{4}He retentivity of all the decays in the apatite and R is the particle radius [2,4]. When the grain radius is larger than 30 μm, F_T is characterized by a rapid rise and gradually approaches 1; however, when the grain radius is smaller than 30 μm, F_T decreases rapidly, and helium is seriously lost. Flowers et al. [8] showed that the apatite He closure temperature had a positive correlation with the grain radius, proven by the apatite He ages from the Otway basin in Australia and the Bighorn Mountains in America [6,12].

Apatite with radius of ~30 μm is defined as the standard sample, with He closure temperature of ~75°C [2–4]. The grain radii of the apatite from the Tarim basin range from 30.6 to 71.5 μm and are larger than ~30 μm (Figure 7). Compared with the standard sample, the apatite from the Tarim basin should accumulated more helium within the same period, which resulted in older apatite He ages and higher apatite He closure temperature.

3.2 Effective uranium concentration (eU)

eU is a concept that has come out in apatite (U-Th)/He thermochronometry in recent years [8,9,21]. eU weights the decay of two parents for their alpha productivity, computed as U+0.23Th [21]. In the current study, the eU of 50 apatite ranges from 1.32 to 181.73 ppm and shows a positive but nonlinear correlation with He ages, similar to the previous studies [8,21] (Figure 8). Shuster et al. [9] analyzed the eU of 3500 apatite from many different rock types and localities and obtained the median value of the eU at 28 ppm in the apatite, defined as a typical apatite. In this paper, the eU of 22 apatite is smaller than 28 ppm, whereas that of the other is greater than 28 ppm, and the individual eU is up to 180 ppm (Figure 8). The He closure temperature for the typical apatite is ~75°C. However, the eU of the apatite is generally higher in the Tarim basin, which may have caused the higher He closure temperature.

The He ages of apatite Z2-1a1 and Z2-1a2 from well Z2 are obviously smaller and deviate from the apatite He partial retention zone in the Tarim basin (Figures 4(a) and 5). The grain radii are 57.5 and 68.3 μm, respectively, larger than ~30 μm, and induce apatite Z2-1a1 and Z2-1a2 to accumulate more helium. However, the eUs of apatite Z2-1a1 and Z2-1a2 are 12.61 and 18.34 ppm, respectively, lower than that of the typical apatite. Therefore, eU is the factor that induces young He ages of apatite Z2-1a1 and Z2-1a2.

3.3 Radiation damage and the radiogenic ^{4}He concentration ([^{4}He])

The radiation damage produced by alpha decay of ^{238}U is defined as the track in apatite fission-track thermochronometry. For slow-cooling terrains, the radiation damage in the apatite can accelerate annealing and result in smaller fission-track ages [9,10]. Farley [11] showed that the He diffusion behavior transition at high temperature coincides closely with progressive annealing of the radiation damage in apatite. As radiation damage accumulates and retards the He diffusion, the apatite yields higher He ages [9,10,17]. Shuster et al. [9] developed a radiation damage trapping model to describe the correlation between radiation damage

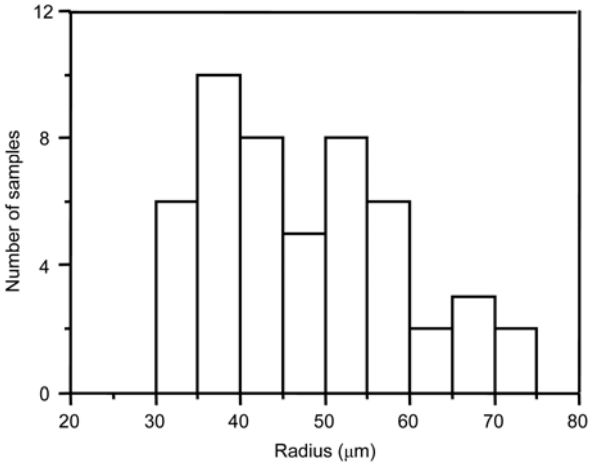

Figure 7 Apatite radii distribution in the Tarim basin.

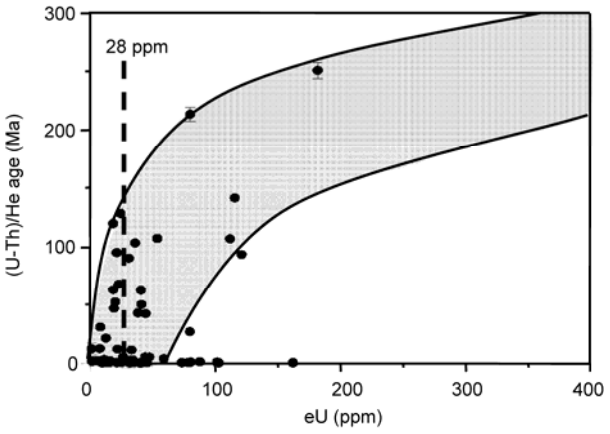

Figure 8 Relationship between eU and apatite He ages in the Tarim basin. The dashed line is the typical eU value of 28 ppm.

and ^{4}He diffusion in which the radiogenic ^{4}He concentration ([^{4}He]) is a proxy of the volume fraction of radiation damage. Radiation damage can trap ^{4}He and improve ^{4}He retention. Samples subjected to reheating after accumulation of substantial radiation damage are more retentive than previously expected [9]. In the Grand Canyon region of the American Colorado Plateau and in the western Canadian Shield, the apatite He ages increase when the radiation damage caused the He retentivity to increase [21–23]. The temperature threshold of radiation damage accumulation in the apatite is ~120°C, much higher than the He closure temperature [9,24]. At temperatures above ~120°C, the radiation damage in apatite greatly diminished and disappeared [9].

The Tabei Uplift, Northern Depression, and Central Uplift in the Tarim basin have been subsiding and have received thick sediments since the Mesozoic. The formation temperature gradually rose but not above ~120°C (the burial depth is shallower than 6000 m). Thus, radiation damage in apatite existed and accumulated in geological time. In the Tarim basin, the long-time radiation damage caused the ^{4}He retentivity and concentration to increase, which finally induced the examined He ages to be much older. A positive but nonlinear correlation between He ages and [^{4}He] is shown in Figure 9. Hence, radiation damage and [^{4}He] also caused the He closure temperature of the apatite in the Tarim basin to increase.

4 Geological significance of apatite He closure temperature

Apatite fission track is the most common method employed in studying the tectono-thermal evolution of the basins and mountains, and its partial annealing zone ranges from 60°C to 125°C [25–30]. In this paper, the He partial retention zone of the apatite in the Tarim basin ranges from 40°C to 88°C. Compared with the apatite fission track, the apatite He ages potentially provide lower temperature thermochronologic constraints and reveal geothermal information of the near surface and the late period of uplift events. For example, the thermal history in some region simulated by the apatite fission track is similar to that shown in Figure 10(a). However, the thermal history simulated by the apatitefission track and (U-Th)/He thermochronometry reveals not only the paths with different cooling rates, as shown in Figure 10(b), but also new tectonic uplifting events, as

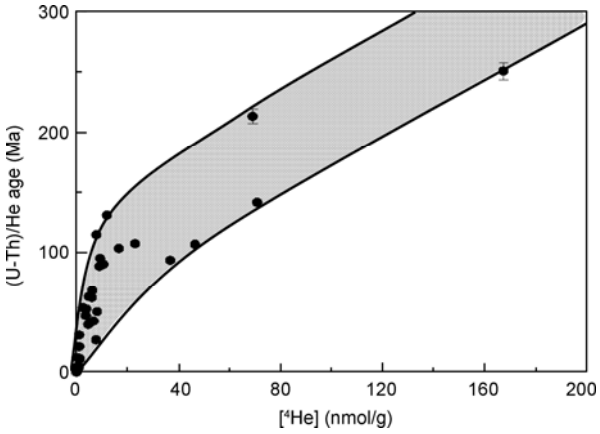

Figure 9 Relationship between [^{4}He] and apatite He ages in the Tarim basin.

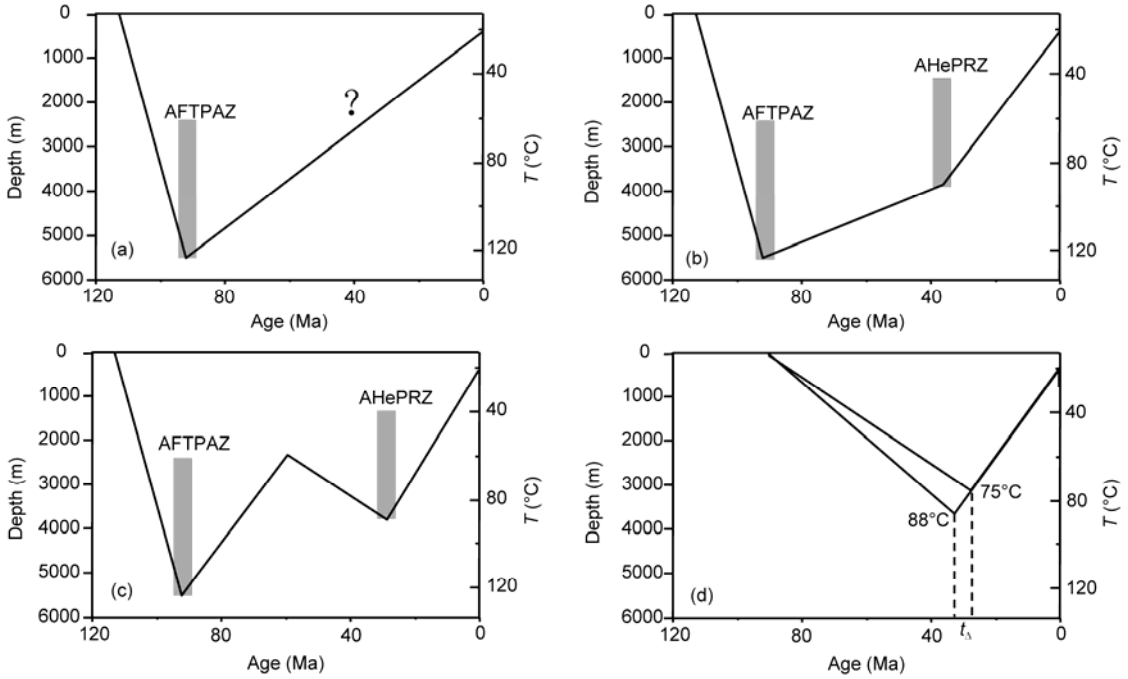

Figure 10 (a) Simulated time-temperature path using the apatite fission-track age; (b) and (c) simulated time-temperature path using the apatite fission track and (U-Th)/He ages; (d) simulated time-temperature paths using the different He closure temperatures. AFTPAZ: Partial annealing zone of the apatite fission track; AHePRZ: He partial retention zone of the apatite.

shown in Figure 10(c). The apatite (U-Th)/He thermochronometry is largely significant in studying the late period of basin-mountain uplifting. Bullen [31] studied the cooling rate of the uplifting event in 3–10 Ma in the Kyrgyz Tianshan using apatite (U-Th)/He thermochronometry and Reiners et al. [31,32] demonstrated the cooling rate of the uplift event in 23–40 Ma in the Dabie Mountain. Recently, we have used the apatite (U-Th)/He ages first to study the South Tianshan and then revealed the rapid uplift during the Neogene [33]. Combined apatite (U-Th)/He and fission track thermochronometries enabled reconstruction of thermal histories between 40°C and 125°C, which provided a better way of studying the thermal histories of basins and mountains [15,19,33–35].

Only suitable apatite He closure temperature contributes to the correct revelation of the time of the last uplift event in a region. Figure 10(d) shows a case where one formation in some regions with the surface temperature of 20°C experienced an uplift event in the geologic time, with an uplift rate of 2°C/Ma. The difference (t_{Δ}) in the initial uplift time, calculated using the He closure temperatures of 88 and 75°C is 6.5 Ma, which is a large uplift time error since the Neogene. Therefore, correctly understanding of the apatite He closure temperature is very important in studying the tectonothermal evolution of basins and mountains.

5 Conclusion

This study has provided the apatite He closure temperature (approximately 88±5°C) of the natural samples in the Tarim basin, which is higher than the 75°C obtained from the thermal simulation experiments, based on the correlation between the apatite He ages and apatite depth in wells S14, S87, S110, XH1, Sh1, Z2, and Z11 in the Tarim basin. The eU, radiation damage, and particle radii induced the increase in the apatite He closure temperature of the Tarim basin. Moreover, the eU and [^{4}He] showed a positive but nonlinear correlation with the apatite He ages in the samples obtained from the Tarim basin. In long-term geological time, the apatite with high eU in the Tarim basin produced more ^{4}He, the radiation damage accumulation retarded the ^{4}He diffusion, and the sufficient grain size retained the ^{4}He. Therefore, the increase in ^{4}He led to the increase in apatite He ages, which resulted in high He closure temperature in the Tarim basin. This study on apatite He closure temperature provides a basis for interpreting the examined He ages in the Tarim basin and has a great significance in studying the uplift events in the Tarim basin and Tianshan.

This work was supported by the National Natural Science Foundation of China (41125010 and 41072103) and the National Basic Research Program of China (2011CB201101). We gratefully thank Prof. P W Reiners in University of Arizona and Dr. S Nicolescu in Yale University who helped a lot in measuring samples and living in America. We also thank Prof. Liu Shaowen and Lei Xiao in Nanjing University for providing the geological data. Finally, we thank the three anonymous reviewers' useful comments and the editor's valuable suggestions for improving this manuscript.

1 Dodson M H. Closure temperature in cooling geochronological and petrological systems. Contrib Mineral Petrol, 1973, 40: 259–274
2 Farley K A, Wolf R A, Silver L T. The effects of long alpha-stopping distances on (U-Th)/He dates. Geochim Cosmochim Acta, 1996, 60: 4223–4229
3 Wolf R A, Farley K A, Silver L T. Helium diffusion and low temperature thermochronometry of apatite. Geochim Cosmochim Acta, 1996, 60: 4231–4240
4 Farley K A. (U-Th)/He dating: Techniques, calibrations, and applications. Rev Mineral Geochem, 2002, 47: 819–844
5 Warnock A C, Zeitler P K, Wolf R A, et al. An evaluation of low-temperature apatite (U-Th)/He thermochronometry. Geochim Cosmochim Acta, 1997, 61: 5371–5377
6 House M A, Farley K A, Kohn B P. An empirical test of helium diffusion in apatite: Borehole data from the Otway basin, Australia. Earth Planet Sci Lett, 1999, 170: 463–474
7 Soderlund P, Juez-Larre J, Page L M, et al. Extending the time range of apatite (U-Th)/He thermochronometry in slowly cooled terranes: Palaeozoic to Cenozoic exhumation history of southeast Sweden. Earth Planet Sci Lett, 2005, 239: 266–275
8 Flowers R M, Ketcham R A, Shuster D L, et al. Apatite (U-Th)/He thermochronometry using a radiation damage accumulation and annealing model. Geochim Cosmochim Acta, 2009, 73: 2347–2365
9 Shuster D L, Flowers R M, Farley K A. The influence of natural radiation damage on helium diffusion kinetics in apatite. Earth Planet Sci Lett, 2006, 249: 148–161
10 Shuster D L, Farley K A. The influence of artificial radiation damage and thermal annealing on helium diffusion kinetics in apatite. Geochim Cosmochim Acta, 2009, 73: 183–196
11 Farley K A. Helium diffusion from apatite: general behavior as illustrated by Durango fluorapatite. J Geophys Res, 2000, 105: 2903–2914
12 Rerners P W, Farley K A. Influence of crystal size on apatite (U-Th)/He thermochronology: An example from the Bighorn Mountains, Wyoming. Earth Planet Sci Lett, 2001, 188: 413–420
13 Qiu N S, Wang J Y, Mei Q H, et al. Constraints of (U-Th)/He ages on early Paleozoic tectonothermal evolution of the Tarim basin, China. Sci China Earth Sci, 2010, 53: 964–976
14 Chang J, Qiu N S, Zuo Y H, et al. The new evidence on tectonic uplift in Kepingtage area, Tarim, China: Constraints from (U-Th)/He ages. Chin J Geophys, 2011, 54: 35–44
15 Qiu N S, Jiang G, Mei Q H, et al. The Paleozoic tectonothermal evolution of the Bachu Uplift of the Tarim basin, NW China: Constraints from (U-Th)/He ages, apatite fission track and vitrinite reflectance data. J Asian Earth Sci, 2011, 41: 551–563
16 Reiners P W. Zircon (U-Th)/He thermochronometry. Rev Mineral Geochem, 2005, 58: 151–179
17 Hendriks B W H, Redfield T F. Apatite fission track and (U-Th)/He data from Fennoscandia: An example of underestimation of fission track annealing in apatite. Earth Planet Sci Lett, 2005, 236: 443–458
18 Green P F, Crowhurst P V, Duddy I R, et al. Conflicting (U-Th)/He and fission track ages in apatite: Enhanced He retention, not anomalous annealing behaviour. Earth Planet Sci Lett, 2006, 250: 407–427
19 Green P F, Duddy I R. Interpretation of apatite (U-Th)/He ages and fission track ages from cratons. Earth Planet Sci Lett, 2006, 244: 541–547
20 Danisik M, Sachsenhofer R F, Privalov V A, et al. Low-temperature thermal evolution of the Azov Massif (Ukrainian Shield-Ukraine) — Implications for interpreting (U-Th)/He and fission track ages from cratons. Tectonophysics, 2008, 456: 171–179
21 Flowers R M, Shuster D L, Wernicke B P, et al. Radiation damage control on apatite (U-Th)/He dates from the Grand Canyon region, Colorado Plateau. Geology, 2007, 35: 447–450
22 Flowers R M. Exploiting radiation damage control on apatite

(U-Th)/He dates in cratonic regions. Earth Planet Sci Lett, 2009, 277: 148–155
23 Flowers R M, Wernicke B P, Farley K A. Unroofing, incision, and uplift history of the southwestern Colorado Plateau from apatite (U-Th)/He thermochronometry. GSA Bull, 2008, 120: 571–587
24 Weber W J, Ewing R C, Meldrum A. The kinetics of alpha-decay-induced amorphization in zircon and apatite containing weapons-grade plutonium or other acinides. J Nucl Mater, 1997, 250: 147–155
25 Cederbom C E, Larson S A, Tullborg E L, et al. Fission track thermochronology applied to Phanerozoic thermotectonic events in central and southern Sweden. Tectonophysics, 2000, 316: 153–167
26 Ren Z L, Xiao H, Liu L, et al. The evidence of fission-track data for the study of tectonic thermal history in Qinshui basin. Chin Sci Bull, 2005, 50(Suppl 1): 104–110
27 Murrell G R, Andriessen P A M. Unraveling a long-term multi-event thermal record in the cratonic interior of southern Finland through apatite fission track thermochronology. Phys Chem Earth, 2004, 29: 695–706
28 Gleadow A J W, Duddy I R, Lovering J F. Fission track analysis: A new tool for the evalution of thermal histories and hydrocarbon potential. APEA, 1983, 23: 93–102
29 Li X M, Wang Y J, Tan K X, et al. Meso-Cenozoic uplifting and exhumation on Yunkaidashan: Evidence from fission track thermochronology. Chin Sci Bull, 2005, 50: 903–909
30 Zhou Z Y, Xu C H, Reiners P W, et al. Late Cretaceous-Cenozoic exhumation history of Tiantangzhai region of Dabieshan Orogen: Constraints from (U-Th)/He and fission track analysis. Chin Sci Bull, 2003, 48: 1151–1156
31 Bullen M E, Burbank D W, Garver J I, et al. Late Cenozoic tectonic evolution of the northwestern Tien Shan: New age estimates for the initiation of mountain building. Geol Soc Amer Bull, 2001, 113: 1544–1559
32 Reiners P W, Zhou Z Y, Ehlers T A, et al. Post-orogenic evolution of the Dabie Shan, Eastern China, from (U-Th)/He and fission track thermochronology. Am J Sci, 2003, 303: 489–518
33 Qiu N S, Chang J, Li J W, et al. New evidence on the Neogene uplift of South Tianshan: Constraints from the (U-Th)/He and AFT ages of borehole samples of the Tarim basin and implications for hydrocarbon generation. Int J Earth Sci, 2012, doi: 10.1007/s00531-011-0745-0
34 Lorencak M, Kohn B P, Osadetz K G, et al. Combined apatite fission and (U-Th)/He thermochronometry in a slowly cooled terrane: Results from a 3440 m deep drill hole in the southern Canadian Shield. Earth Planet Sci Lett, 2004, 227: 87–104
35 Hansen K, Reiners P W. Low temperature thermochronology of the southern East Greenland continental margin: Evidence from apatite (U-Th)/He and fission track analysis and implications for intermethod calibration. Lithos, 2006, 92: 117–136